GEOPHYSICS, VOL. 73, NO. 2 (MARCH-APRIL 2008); P. U1–U11, 10 FIGS., 5 TABLES.
10.1190/1.2834115

AVO-sensitive semblance analysis for wide-azimuth data

Jia Yan[1] and Ilya Tsvankin[1]

ABSTRACT

Conventional semblance-based moveout analysis models prestack reflection data with events that have hyperbolic moveout and no amplitude variation with offset (AVO). Substantial amplitude variation and even phase change with offset do not significantly compromise the semblance operator. However, polarity reversal associated with a change in the sign of the reflection coefficient may cause conventional semblance to fail. An existing modification of the semblance operator that takes amplitude variations into account (so-called AK semblance) is limited to narrow-azimuth data and cannot handle nonhyperbolic moveout at large offsets. We employ a 3D nonhyperbolic moveout inversion algorithm to extend the AK semblance method to wide-azimuth data recorded on long spreads. To preserve velocity resolution, the ratio K of the AVO gradient and intercept is kept constant within each semblance window. In the presence of azimuthal anisotropy, however, the parameter K has to be azimuthally dependent. Synthetic tests confirm that distortions in moveout analysis caused by polarity reversals become more common for long-offset data. Conventional semblance produces substantial errors in the NMO ellipse and azimuthally varying anellipticity parameter η not just for class 2 AVO response but also for some models with class 1 AVO. In contrast, the AK semblance algorithm gives accurate estimates of the moveout parameters even when the position of the polarity reversal varies with azimuth. The AK method not only helps to flatten wide-azimuth reflection events prior to stacking and azimuthal AVO analysis but also provides input parameters for the anisotropic geometrical-spreading correction.

INTRODUCTION

Semblance-based moveout analysis is routinely used in seismic data processing to estimate stacking (moveout) velocity V_{nmo} as a function of zero-offset time t_0 (e.g., Taner and Koehler, 1969). The moveout velocity, which typically represents the most stable parameter constrained by surface seismic data, is then used to build the initial velocity model and flatten reflection events for subsequent processing (e.g., stacking, AVO analysis).

The conventional semblance operator can be written as

$$S(V,t_0) = \frac{\sum\limits_{t_1}\left[\sum\limits_{x} D_V(t_1,x)\right]^2}{N\sum\limits_{t_1}\sum\limits_{x} D_V^2(t_1,x)}, \qquad (1)$$

where t_1 are the zero-offset times within a time window centered at t_0, x is the source-to-receiver offset, N is the number of traces in a common-midpoint (CMP) gather, and D_V represents the data along hyperbolic moveout curves computed with the velocity $V = V_{\mathrm{nmo}}$.

Despite its general robustness, conventional semblance computation has two serious limitations. First, the semblance operator 1 is devised under the assumption that reflection amplitudes are constant; therefore, it includes no allowance for amplitude variation with offset (AVO). Still, conventional semblance usually estimates moveout velocity with sufficient accuracy, even for events with relatively strong AVO, as long as there is no polarity reversal within the recorded offset range. In the presence of polarity reversals, however, the conventional operator often fails and gives a strongly distorted NMO-velocity value (Sarkar et al., 2001). Then the reflection event cannot be properly flattened, which leads to a poor-quality, low-frequency stack.

Second, most existing implementations of semblance analysis do not account for deviations from hyperbolic moveout, which become significant for offset-to-depth ratios greater than unity. To make equation 1 suitable for long-spread reflection events, the hyperbolic moveout equation can be replaced by more complicated nonhyperbolic functions, such as those developed for layered anisotropic media by Tsvankin and Thomsen (1994) and Alkhalifah and Tsvankin

Manuscript received by the Editor 23 July 2007; revised manuscript received 18 October 2007; published online 4 March 2008.
[1]Colorado School of Mines, Department of Geophysics, Center for Wave Phenomena, Golden, Colorado, U.S.A. E-mail: jyan@dix.mines.edu; ilya@dix.mines.edu.

(1995). A detailed discussion of nonhyperbolic moveout analysis can be found in Tsvankin (2005).

Figure 1 displays three common classes of P-wave AVO behavior for gas sands described in Rutherford and Williams (1989). Classes 1 and 2 correspond to highly or moderately compressed sands beneath shales; class 3 sands are overlain by a more compressed overburden. For class 1 and class 2 responses, a polarity reversal occurs at incidence angles less than 30°. Furthermore, the influence of anisotropy increases the chance of observing polarity reversals on conventional-spread reflection data. Indeed, most shale formations are transversely isotropic (TI), and for typical positive values of the Thomsen (1986) parameter δ in shales, the AVO gradient increases by absolute value (Kim et al., 1993; Tsvankin, 2005). As a result, the polarity reversal for gas sands overlain by VTI (TI with a vertical symmetry axis) shales moves toward lower angles from its "isotropic" position (Figure 1).

To make moveout analysis suitable for data with polarity reversals, Sarkar et al. (2002) have developed the so-called AK semblance method. Their approach is based on introducing into the semblance operator a smooth amplitude variation with offset governed by two parameters, A and K. The existing AK algorithm, however, is restricted to 2D data and the hyperbolic portion of the moveout curve (i.e., to moderate-length spreads).

Other alternatives to conventional semblance designed to correct for AVO include the eigenvalue method (Biondi and Kostov, 1989; Key and Smithson, 1990) and differential semblance analysis (Symes and Kern, 1994). However, these techniques have serious shortcomings, discussed in detail by Sarkar et al. (2001).

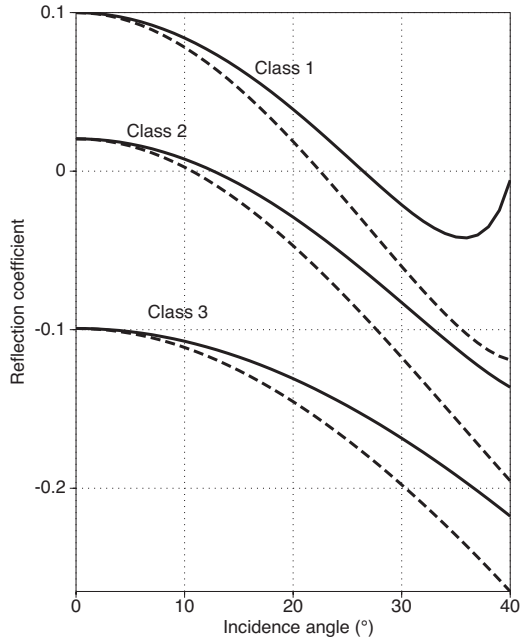

Figure 1. Three classes of P-wave AVO responses (reflection coefficients) computed from exact equations (e.g., Rüger, 2001) for gas sands overlain by shale. The solid lines correspond to the three isotropic models from Table 1 (Rutherford and Williams, 1989). The dashed lines are computed for models with the same vertical velocities and densities, but the shale layer is VTI with the Thomsen parameters $\varepsilon = \delta = 0.2$. All three models have negative AVO gradients, which become larger by absolute value when the shale is anisotropic.

Here, we present an extension of the AK semblance method to wide-azimuth, long-offset data. Our generalized AK algorithm is particularly important for processing reflection data from anisotropic media because anisotropy usually moves the polarity reversal toward smaller offsets (see above) and enhances nonhyperbolic moveout of P-waves (Tsvankin, 2005). Also, azimuthally varying polarity reversals may substantially distort the results of moveout analysis for wide-azimuth surveys acquired above fractured formations. Vasconcelos and Tsvankin (2006) present an efficient technique for nonhyperbolic moveout inversion of wide-azimuth data from layered azimuthally anisotropic media, but their semblance operator does not take amplitude variations into account.

We begin by reviewing the AK semblance algorithm of Sarkar et al. (2002) and its implementation in moveout analysis. Then we show that the AK semblance operator can be extended to long-offset 2D data from layered VTI or isotropic media using the nonhyperbolic moveout equation of Alkhalifah and Tsvankin (1995). To apply the method to wide-azimuth reflection events, we make the AVO gradient azimuthally dependent and incorporate it into the moveout-inversion algorithm of Vasconcelos and Tsvankin (2006). Synthetic tests for VTI and azimuthally anisotropic (orthorhombic) models demonstrate the superior performance of the generalized AK semblance for both class 1 and class 2 AVO responses.

METHODOLOGY

As discussed above, the conventional semblance operator in equation 1 does not account for amplitude variations within the CMP gather. A more general semblance formulation for 2D data is introduced by Corcoran and Seriff (1993) and Sarkar et al. (2002):

$$S_G(V,t_0) = 1 - \frac{\|M - D_V\|^2}{\|D_V\|^2}, \qquad (2)$$

where t_0, as before, is the zero-offset time at the center of the semblance window, $D_V = D_V(t_1,x)$ is the data with the zero-offset time t_1 after a hyperbolic moveout correction with the velocity $V = V_{\mathrm{nmo}}$, and $M = M(t_1,x)$ is the modeled variation of the trace amplitudes. The velocity V_{nmo} and the amplitude parameters that govern $M(t_1,x)$ are estimated by matching the model M and data D, which can be achieved by maximizing the semblance (i.e., by minimizing $\|M - D_V\|^2$). The generalized semblance from equation 2 reduces to the conventional semblance operator (equation 1) when the amplitudes associated with model M are independent of offset (Sarkar et al., 2002).

The offset-dependent function M in the AVO-sensitive semblance algorithm can be approximately described by Shuey's (1985) linearized equation for the plane P-wave reflection coefficient:

Table 1. Model parameters for the three classes of AVO responses in Figure 1.

		V_P (km/s)	V_S (km/s)	ρ (g/cm^3)
Layer 1		3.00	1.32	2.4
Layer 2	Class 1	4.40	2.80	2.0
	Class 2	3.75	2.40	2.0
	Class 3	2.95	1.89	2.0

$$M(t_1,x) = A(t_1) + B(t_1)\sin^2\theta_x \approx A(t_1) + B(t_1)\frac{x^2}{x^2 + t_0^2 V_{\rm nmo}^2}, \quad (3)$$

where $A(t_1)$ and $B(t_1)$ are the AVO intercept and gradient (respectively) for the reflection event with the zero-offset time t_1, and θ_x is the phase angle of incidence, which is expressed through offset x under the assumption that the medium is homogeneous and isotropic. The exact incidence angle θ_x cannot be computed without knowledge of the velocity model. It should be emphasized, however, that there is no need for an accurate estimate of θ_x because equation 3 is designed exclusively to introduce a smooth amplitude variation with offset into the semblance operator. Note that Shuey's (1985) equation cannot represent measured reflection amplitudes anyway because it does not include source directivity and propagation factors such as the geometrical spreading and transmission coefficients.

As pointed out by Sarkar et al. (2002), equation 3 (called AB semblance) allows too much freedom to fit events with various combinations of incorrect parameters A, B, and $V_{\rm nmo}$, which results in poor velocity resolution. To reduce the trade-offs between A, B, and $V_{\rm nmo}$, Sarkar et al. (2002) suggest keeping the ratio $B/A = K$ constant inside the semblance window, which implies that the wavelet shape does not change with offset:

$$M(t_1,x) = A(t_1)\left(1 + K\frac{x^2}{x^2 + t_0^2 V_{\rm nmo}^2}\right). \quad (4)$$

Modeling data using equation 4 with a constant K is referred to by Sarkar et al. (2002) as AK semblance.

The semblance window follows the traveltime trajectory computed from an analytic (hyperbolic in the work by Sarkar et al., 2002) moveout equation and has the width close to the length of the wavelet. For a window with N_t sampling points, the AK semblance operator has only $N_t + 1$ parameters (as compared with $2N_t$ for AB semblance), which mitigates the trade-offs and increases velocity resolution.

For a given zero-offset time t_0 and a trial velocity $V_{\rm nmo}$, the parameters A and K can be found analytically by setting the derivatives of S_G with respect to A and K to zero (see Appendix A). The obtained expressions are then substituted back into equation 2 to compute the generalized AK semblance. As in conventional semblance algorithms, scanning over $V_{\rm nmo}$ is used to maximize the semblance and estimate the best-fit moveout (stacking) velocity.

A key issue in implementing the generalized semblance algorithm is the choice of the moveout equation $t(x)$. Reflection moveout on conventional-length spreads (i.e., for offset-to-depth ratios not much larger than unity) typically is close to hyperbolic:

$$t^2(x) = t_0^2 + \frac{x^2}{V_{\rm nmo}^2}. \quad (5)$$

Although equation 5 is widely used in seismic processing, it breaks down at longer offsets, especially if the medium is anisotropic. A more accurate, nonhyperbolic moveout equation for P-wave data in VTI media is suggested by Alkhalifah and Tsvankin (1995):

$$t^2(x) = t_0^2 + \frac{x^2}{V_{\rm nmo}^2} - \frac{2\eta x^4}{V_{\rm nmo}^2\left[t_0^2 V_{\rm nmo}^2 + (1 + 2\eta)x^2\right]}, \quad (6)$$

where $\eta \equiv (\varepsilon - \delta)/(1 + 2\delta)$ is the anellipticity parameter, which controls P-wave time processing for vertical transverse isotropy. The x^4-term in equation 6 is proportional to η and describes nonhyperbolic moveout for large offsets. Below, we use the Alkhalifah-Tsvankin equation in the AK semblance operator to perform moveout analysis of 2D long-spread P-wave data.

The main goal of the paper, however, is to extend the principle of AK semblance to wide-azimuth surveys, which are often acquired for purposes of fracture detection or better illumination of complicated subsurface structures (e.g., in subsalt exploration). Reservoirs with vertical fracture sets are commonly described by an effective anisotropic model with orthorhombic symmetry (Schoenberg and Helbig, 1997; Bakulin et al., 2000; Grechka and Kachanov, 2006). Azimuthally dependent P-wave reflection traveltimes in a horizontal orthorhombic layer can be well-approximated by a generalized version of equation 6, in which both the NMO velocity and parameter η vary with azimuth α (Xu and Tsvankin, 2006a; Vasconcelos and Tsvankin, 2006):

$$t^2(x,\alpha) = t_0^2 + \frac{x^2}{V_{\rm nmo}^2(\alpha)} - \frac{2\eta(\alpha)x^4}{V_{\rm nmo}^2(\alpha)\left[t_0^2 V_{\rm nmo}^2(\alpha) + (1 + 2\eta(\alpha))x^2\right]}. \quad (7)$$

The velocity $V_{\rm nmo}$ is obtained from the equation of the NMO ellipse:

$$V_{\rm nmo}^{-2}(\alpha) = \frac{\cos^2(\alpha - \varphi)}{[V_{\rm nmo}^{(2)}]^2} + \frac{\sin^2(\alpha - \varphi)}{[V_{\rm nmo}^{(1)}]^2}, \quad (8)$$

where φ is the azimuth of the $[x_1,x_3]$ symmetry plane, and $V_{\rm nmo}^{(1)}$ and $V_{\rm nmo}^{(2)}$ are the NMO velocities in the symmetry planes $[x_2,x_3]$ and $[x_1,x_3]$, respectively. (The superscripts in $V_{\rm nmo}^{(1)}$ and $V_{\rm nmo}^{(2)}$ refer to the axis orthogonal to the corresponding plane; for a detailed discussion of notation, see Tsvankin [1997, 2005]). The azimuthal variation of the parameter η is given approximately by (Pech and Tsvankin, 2004):

$$\eta(\alpha) = \eta^{(2)}\cos^2(\alpha - \varphi) + \eta^{(1)}\sin^2(\alpha - \varphi) - \eta^{(3)}\cos^2(\alpha - \varphi)\sin^2(\alpha - \varphi), \quad (9)$$

where $\eta^{(1)}$, $\eta^{(2)}$, and $\eta^{(3)}$ are the anellipticity parameters defined (respectively) in the $[x_2,x_3]$, $[x_1,x_3]$, and $[x_1,x_2]$ symmetry planes.

The accuracy of equation 7 in both vertical symmetry planes is the same as that in the corresponding equivalent VTI medium. Xu and Tsvankin (2006a) and Vasconcelos and Tsvankin (2006) show that equations 7–9 provide a close approximation for long-spread P-wave traveltimes recorded in all azimuthal directions, even for strongly anisotropic orthorhombic models. Furthermore, if $V_{\rm nmo}^{(1,2)}$ and $\eta^{(1,2,3)}$ are treated as effective parameters, the same formalism can be applied to P-wave moveout from layered orthorhombic media with uniform orientation of the symmetry planes.

Vasconcelos and Tsvankin (2006) use equations 7–9 to develop an efficient semblance-based moveout-inversion algorithm designed to estimate the parameters φ, $V_{\rm nmo}^{(1,2)}$, and $\eta^{(1,2,3)}$ from wide-azimuth P-wave data. Their method, however, does not account for amplitude variation with offset and azimuth and, similar to conventional 2D semblance techniques, can break down in the presence of polari-

ty reversals. Below, we devise a more stable, 3D AK semblance operator by incorporating an azimuthally dependent amplitude function into the semblance computation.

When the medium above or below the reflector is azimuthally anisotropic, the AVO gradient and reflection amplitude as a whole vary with azimuth. For a boundary between two orthorhombic half-spaces with the same orientation of the vertical symmetry planes, the AVO gradient $B(\alpha)$ can be approximated by (Rüger, 2001)

$$B(\alpha) = B^{(1)} \sin^2(\alpha - \varphi) + B^{(2)} \cos^2(\alpha - \varphi); \quad (10)$$

$B^{(1)}$ and $B^{(2)}$ are the AVO gradients in the $[x_2,x_3]$ and $[x_1,x_3]$ planes, respectively. Then the ratio $K(\alpha)$ of the AVO gradient and intercept also becomes azimuthally dependent and can be written as

$$K(\alpha) = K^{(1)} \sin^2(\alpha - \varphi) + K^{(2)} \cos^2(\alpha - \varphi), \quad (11)$$

where $K^{(1)} = B^{(1)}/A$ and $K^{(2)} = B^{(2)}/A$. Substituting $K(\alpha)$ from equation 11 into equation 4 yields an azimuthally dependent amplitude function that can be used in the AK semblance computation:

$$M(t_1,x,\alpha) = A(t_1)\left\{1 + [K^{(1)} \sin^2(\alpha - \varphi) + K^{(2)} \cos^2(\alpha - \varphi)] \frac{x^2}{x^2 + t_0^2 V_{\mathrm{nmo}}^2(\alpha)}\right\}. \quad (12)$$

In our method, we combine the amplitude function 12 with the moveout equations 7–9 to devise an AK semblance operator that can handle polarity reversals in wide-azimuth data collected into CMP gathers (see Appendix A). Although this formalism does not account for geometrical spreading and some other factors that influence recorded amplitudes, equation 12 allows us to correct for amplitude variation with offset and azimuth. In particular, our operator mitigates distortions in the semblance computation related to the azimuthal dependence of the offset that corresponds to the polarity reversal.

Similar to the algorithm of Vasconcelos and Tsvankin (2006), we estimate $K^{(1)}$, $K^{(2)}$, and the moveout parameters φ, $V_{\mathrm{nmo}}^{(1,2)}$, and $\eta^{(1,2,3)}$ in three steps. (As in 2D, $A(t_1)$ is obtained analytically.) First, we invert for the NMO ellipse described by φ, $V_{\mathrm{nmo}}^{(1)}$, and $V_{\mathrm{nmo}}^{(2)}$ using conventional-spread, wide-azimuth data with offsets limited by the reflector depth. If there is an indication of a polarity reversal at the near offsets, we also estimate an azimuthally invariant value of K along with the NMO ellipse. This step gives initial values of the symmetry-plane azimuths, NMO velocities, and the parameter K.

Second, 2D nonhyperbolic AK semblance analysis is carried out in narrow azimuthal sectors around the identified symmetry planes to find approximate values of $\eta^{(1)}$, $\eta^{(2)}$, $K^{(1)}$, and $K^{(2)}$, as well as updated estimates of $V_{\mathrm{nmo}}^{(1)}$ and $V_{\mathrm{nmo}}^{(2)}$. Third, we carry out 3D nonhyperbolic moveout inversion using the 3D AK semblance operator for all offsets and azimuths in the gather.

The 3D search starts with the initial model obtained during the previous steps and estimates the best-fit parameters φ, $V_{\mathrm{nmo}}^{(1,2)}$, $\eta^{(1,2,3)}$, and $K^{(1,2)}$ (i.e., the parameters that give the highest semblance value) via Powell minimization. The Powell method (Press et al., 1992) is a multidimensional search algorithm designed to find the local minimum of the objective function closest to the initial model. In general, there is no guarantee that this method can find the global minimum, which in our case corresponds to the model with the largest semblance value. However, because of the high accuracy of our initial model obtained from the first two inversion steps, the algorithm typically converges to the global minimum after 10–20 iterations.

It should be emphasized that the method can handle vertically heterogeneous media composed of isotropic, VTI, HTI (TI with a horizontal symmetry axis), and orthorhombic layers. The vertical symmetry planes in all azimuthally anisotropic layers, however, have to be aligned. Otherwise, the azimuthally dependent parameter $\eta(\alpha)$ is not co-oriented with the NMO ellipse, and equation 9 has to be modified (Vasconcelos and Tsvankin, 2006; Xu and Tsvankin, 2006a).

TESTS ON SYNTHETIC DATA

Here, the AK semblance algorithm is applied to 2D and 3D long-offset P-wave data from VTI and orthorhombic media. In addition to class 2 AVO responses, for which the polarity reversal is observed at relatively small offsets, we compare the performance of conventional and AK semblance for class 1 AVO. All synthetic data used below are generated by the anisotropic ray-tracing code ANRAY developed by Gajewski and Pšenčík (1987). Although tests on noise-contaminated data are left out, our algorithm (as any other semblance-based method) is not sensitive to random noise.

2D semblance for VTI media

For layer-cake VTI media, each vertical plane is a plane of symmetry, and semblance analysis can be performed in 2D for an arbitrary azimuthal direction of the acquisition line. We consider a model that includes an isotropic half-space beneath a VTI layer with relatively small absolute values of the Thomsen parameters ε and δ (Table 2). The anellipticity parameter η, however, is substantial (0.2), which leads to pronounced nonhyperbolic moveout at offsets approaching two reflector depths. The event has a class 2 AVO response (see the discussion above), with relatively low amplitudes at near offsets and a polarity reversal at an offset close to half the reflector depth (Figure 2).

The first test was carried out using the hyperbolic moveout equation in both the conventional and AK semblance operators (Figure 3). Because of the combined influence of the polarity reversal and nonhyperbolic moveout, the conventional operator produces low semblance values for all trial velocities, with the correct velocity close to the semblance minimum. Although the AK algorithm performs much better and yields higher semblance, the best-fit NMO velocity deviates from the actual value. This error, which is caused by the inaccuracy of the hyperbolic moveout equation, can be reduced by muting out long offsets.

However, in such applications as nonhyperbolic moveout inversion and wide-angle AVO

Table 2. Parameters of a model that includes VTI (top) and isotropic (ISO; bottom) media. The P-wave reflection for this model has a class 2 AVO response. The vertical P- and S-wave velocities, respectively, are V_{P0} and V_{S0}.

	V_{P0} (km/s)	V_{S0} (km/s)	ρ (g/cm^3)	ε	δ	V_{nmo} (km/s)	η
VTI	2.96	1.38	2.43	0.065	−0.096	2.66	0.2
ISO	3.49	2.29	2.14	0	0	3.49	0

analysis, it is necessary to preserve and flatten the far-offset portion of the gather. The traveltime fit at long offsets can be improved by using the nonhyperbolic moveout equation 6 in the semblance computation (Figure 4). Although equation 6 provides a close approximation to the exact long-spread traveltimes (Alkhalifah and Tsvankin, 1995; Tsvankin, 2005), the best-fit parameters V_{nmo} and η estimated by the conventional semblance algorithm are severely distorted (e.g., the inverted $\eta = 0.72$, whereas the actual value is 0.2). Clearly, this error is caused by the polarity reversal because the semblance that corresponds to the correct moveout parameters is relatively low. In contrast, AK semblance gives accurate estimates of both V_{nmo} and η, as well as a high semblance value (0.94).

3D semblance for class 2 AVO

Here, we apply the 3D AK semblance operator to wide-azimuth P-wave reflections from the bottom of an orthorhombic layer. The AVO gradient for this model is azimuthally dependent, so the offset of the polarity reversal becomes a function of azimuth as well. If the polarity reversal occurs at relatively small offsets, the corresponding phase incidence angle θ_{pr} can be estimated by setting $1 + K(\alpha)\sin^2\theta_{pr} = 0$. Using equation 11 with $\varphi = 0$ (i.e., zero azimuth corresponds to the $[x_1,x_3]$-plane), we find

$$\sin^2\theta_{pr} = \frac{-1}{K^{(1)}\sin^2\alpha + K^{(2)}\cos^2\alpha}. \qquad (13)$$

If the medium above the reflector is homogeneous and the difference between the group and phase angles can be neglected, equation 13 provides an estimate of the offset x_{pr} of the polarity reversal:

$$\frac{x_{pr}(\alpha)}{h} \approx 2\tan\theta_{pr} = \frac{2}{\sqrt{-\left(1 + K^{(1)}\sin^2\alpha + K^{(2)}\cos^2\alpha\right)}}, \qquad (14)$$

where h is the reflector depth.

Model 1

The first test was performed for a boundary between orthorhombic (top) and isotropic (bottom) half-spaces (Figure 5). Both media have the same vertical velocities and densities as those in the VTI/isotropic model analyzed above (see Table 2 and Figures 2–4). Also, the anisotropy parameters in the symmetry plane $[x_1,x_3]$ of the orthorhombic medium are taken from the VTI model in Table 2. Although the medium above the reflector is azimuthally anisotropic, the offset of the polarity reversal is weakly dependent on azimuth (Figure 5).

The initial model for 3D analysis of the long-spread gather was obtained by first estimating the NMO ellipse on conventional-spread data and then processing long-offset data (in 2D, for the maximum offset-to-depth ratio $x_{max}/h = 2$) within narrow sectors centered at the vertical symmetry planes. The NMO ellipse reconstructed by the conventional semblance operator for offset-to-depth ratios limited by unity has the correct orientation but highly distorted semiaxes equal to 3.20 and 3.44 km/s (the actual values are 2.66 and 2.87 km/s); the semblance is only 0.45. Therefore, for class 2 AVO with small values of x_{pr}, muting out long offsets does not help the conventional algorithm

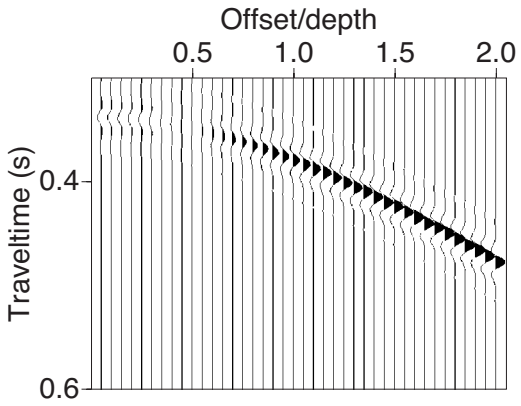

Figure 2. Shot record of a P-wave reflection from an interface between VTI (top) and isotropic (bottom) media. The model parameters are listed in Table 2. The event has a class 2 AVO response with the polarity reversal at an offset-to-depth ratio close to 0.5.

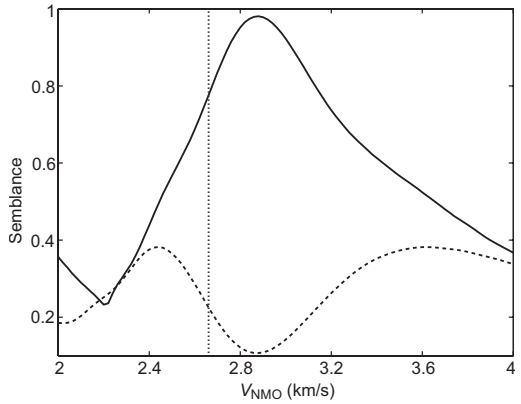

Figure 3. Semblance for the reflection event from Figure 2 computed using the hyperbolic moveout equation 5; the model parameters are listed in Table 2. The dashed curve is produced by the conventional semblance algorithm, and the solid curve is AK semblance. The vertical dotted line marks the actual NMO velocity.

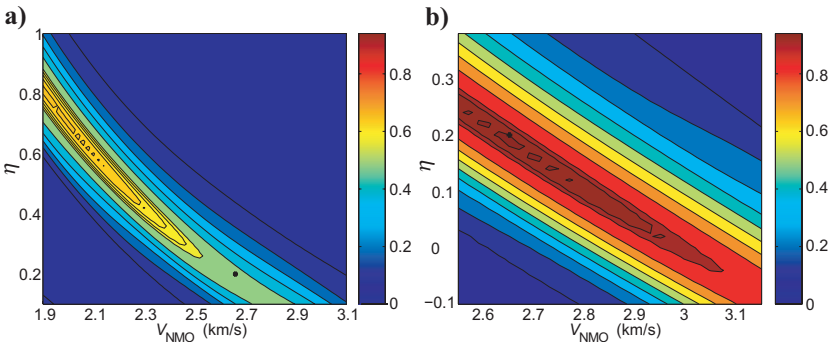

Figure 4. Semblance scans over V_{nmo} and η computed for the event from Figure 2 using the nonhyperbolic moveout equation 6. The scans are generated by the (a) conventional and (b) AK semblance operators. The black dots mark the actual model parameters, $V_{nmo} = 2.66$ km/s and $\eta = 0.2$. The best-fit values are $V_{nmo} = 1.98$ km/s and $\eta = 0.72$ for conventional semblance (the maximum semblance is 0.72) and $V_{nmo} = 2.68$ km/s, $\eta = 0.18$ for AK semblance (the maximum semblance is 0.94).

estimate the NMO ellipse. Clearly, for this model, conventional processing cannot be used for stacking or moveout inversion of wide-azimuth data.

The final inversion results for two spreadlengths ($x_{max}/h = 2$ and $x_{max}/h = 3$) are displayed in Figure 6. Note that with both conventional and AK semblance, the parameters for the $[x_1,x_3]$ symmetry plane estimated from the 3D inversion almost coincide with those obtained for the VTI model in Figure 4. Because of the influence of the polarity reversal, conventional semblance produces large errors in the NMO velocities and η values for both spreadlengths. As was the case for the VTI model, AK semblance correctly compensates for the polarity reversal and gives accurate estimates of the azimuthally varying parameters V_{nmo} and η.

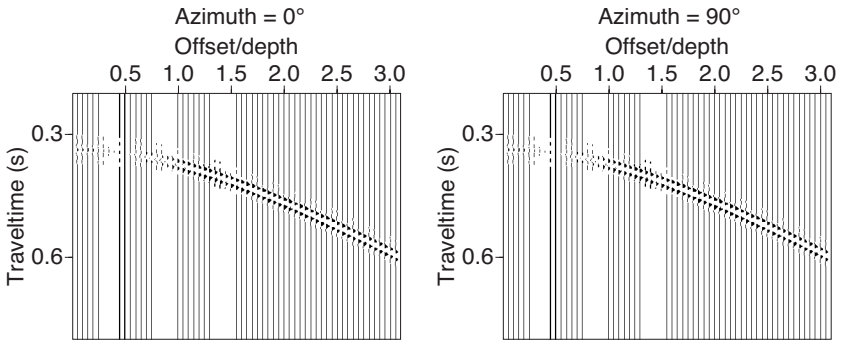

Figure 5. Shot records of a P-wave reflection from an orthorhombic/isotropic interface with a type 2 AVO response (Table 3). The seismograms are computed for the symmetry planes $[x_1,x_3]$ (azimuth $\alpha = 0°$) and $[x_2,x_3]$ ($\alpha = 90°$).

Table 3. Parameters of a model that includes orthorhombic (top) and isotropic (bottom) media. The P-wave reflection from this interface has an azimuthally varying class 2 AVO response. The notation for orthorhombic media is discussed in Tsvankin (1997, 2005).

	Layer 1	Layer 2
Symmetry type	ORTH	ISO
Density (g/cm^3)	2.43	2.14
V_{P0} (km/s)	2.96	3.49
V_{S0} (km/s)	1.38	2.29
$\varepsilon^{(1)}$	0.065	0
$\delta^{(1)}$	−0.029	0
$\gamma^{(1)}$	0.18	0
$\varepsilon^{(2)}$	0.065	0
$\delta^{(2)}$	−0.096	0
$\gamma^{(2)}$	0.05	0
$\delta^{(3)}$	−0.08	0
$V_{nmo}^{(1)}$	2.87	3.49
$V_{nmo}^{(2)}$	2.66	3.49
$\eta^{(1)}$	0.10	0
$\eta^{(2)}$	0.20	0
$\eta^{(3)}$	0.10	0

Model 2

In the next test, we use another class 2 AVO model (Table 4), for which the offset x_{pr} of the polarity reversal is larger and varies more strongly with azimuth (Figure 7). The normalized offset x_{pr}/h changes from 0.65 in the $[x_1,x_3]$ symmetry plane ($\alpha = 0°$) to 0.85 in the $[x_2,x_3]$-plane ($\alpha = 90°$).

The NMO ellipse reconstructed by the conventional method for offsets limited by the reflector depth has the correct orientation and the semiaxes 2.43 and 2.11 km/s (actual values are 2.53 and 2.16 km/s); the semblance is 0.6. The better performance of the conventional method for model 2 is explained by the relatively large (for class 2 AVO) offset $x_{pr}(\alpha)$ of the polarity reversal and low reflection amplitudes for $x > x_{pr}$.

Application of the AK algorithm, however, becomes necessary for long-offset data because conventional semblance yields highly erroneous η values (Figure 8b and d). As discussed above, we obtain the initial model for 3D analysis by first estimating the NMO ellipse on conventional-spread data with $K^{(1)} = K^{(2)} = K$ and then processing long-offset data near the vertical symmetry planes to give $K^{(1)} = -5.85$ and $K^{(2)} = -6.21$.

The results of 3D nonhyperbolic AK semblance analysis for two long spreads are shown in Figure 8. The polarity reversal now occurs at offsets smaller than one-half of the spreadlength, so conventional semblance produces a significant error not only in η but also in the NMO ellipse. The η values estimated by the conventional algorithm for $x_{max}/h = 2$ even become negative for a wide range of azimuths (Figure 8b).

The AK semblance method, which properly accounts for the azimuthally dependent polarity reversal, gives far superior results. There is practically no error in the NMO ellipse, whereas the mild distortion in η for $x_{max}/h = 2$ is caused by the small bias in the nonhyperbolic moveout equation (Tsvankin, 2005) and insufficient spreadlength. When the maximum offset-to-depth ratio is increased from two to three (Figure 8d), the errors in the function $\eta(\alpha)$ become almost negligible.

3D semblance for class 1 AVO

Compared to the class 2 AVO response analyzed, class 1 AVO is typically characterized by a higher normal-incidence reflection coefficient, and the polarity reversal is observed at larger offsets (Figure 1). As long as the polarity reversal occurs outside the recorded offset range or near the end of the spread, the data can be processed by the conventional semblance algorithm. However, for events with offset-to-depth ratios reaching two, the offset x_{pr} may be close to the middle of the spread. In addition, anisotropy tends to move the polarity reversal toward smaller offsets (Figure 1).

Figure 9 displays a long-spread P-wave reflection from an interface between orthorhombic and isotropic media (Table 5). The event has a typical class 1 AVO response, with the polarity reversal recorded at offset-to-depth ratios of about 1.2. Although the conventional algorithm performs better than it did for class 2 AVO, the errors in both the NMO ellipse and parameter η are substantial (Figure 10). A more accurate reconstruction of the NMO ellipse using conventional semblance can be achieved by reducing the maximum offset-to-

depth ratio to $x_{max}/h < 1.2$ (i.e., by truncating the spread before the polarity reversal). Despite the presence of the polarity reversal, the error in the NMO ellipse obtained by the AK semblance is almost negligible for both spreadlengths (Figure 10a and c).

As was the case for class 2 AVO (see Figure 8), the AK semblance operator gives a higher accuracy in η for the longer spread ($x_{max}/h = 3$), especially in the $[x_1,x_3]$-plane where $\eta(\alpha)$ reaches its maximum (Figure 10b and d). Somewhat suprisingly, the η estimate produced by the conventional semblance deteriorates with increasing spreadlength. This reduction in accuracy is most likely explained by the increased distortion caused by the polarity reversal on longer spreads, as the semblance becomes more influenced by traces at large (postreversal) offsets $x > x_{pr}$.

DISCUSSION

Our results demonstrate that a smooth amplitude function based on Shuey's equation for the AVO gradient is sufficient for removing the influence of polarity reversals on semblance analysis. Still, it should be emphasized that AK semblance should not be regarded as a substitute for 2D or 3D (azimuthal) AVO analysis. Whereas the small-offset AVO equation used in our algorithm is sufficient to correct for the phase change of the wavelet in the presence of polarity reversals, it does not properly account for higher-order AVO terms.

Also, the obtained value of K is distorted by propagation phenomena, such as the geometrical spreading and transmission coefficients

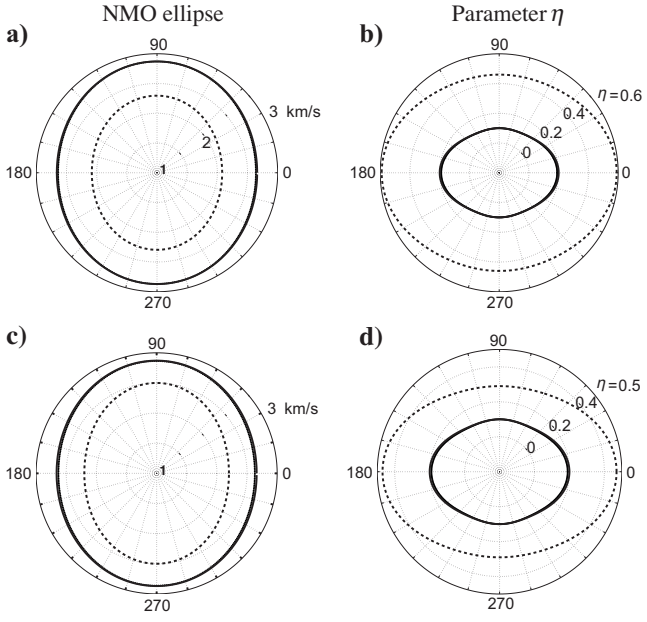

Figure 6. Moveout-inversion results for a wide-azimuth, long-offset P-wave reflection from an orthorhombic/isotropic interface (Table 3). The event has a class 2 AVO response with the polarity reversal at offset-to-depth ratios close to 0.5 (Figure 5). (a) and (c) are the NMO ellipses; (b) and (d) are the azimuthally dependent η values. The maximum offset-to-depth ratio is two for the top row (a and b) and three for the bottom row (c and d). The solid lines are the actual NMO ellipses and η-curves, the dashed lines are estimated by the conventional semblance algorithm, and the dotted lines by AK semblance. Since the AK semblance algorithm reconstructs the moveout parameters with high accuracy, the dotted and solid lines almost coincide. The azimuth with respect to the symmetry plane $[x_1,x_3]$ is shown on the perimeter.

along the raypath. Therefore, the role of the AK semblance method is limited to estimating an accurate set of parameters that control the nonhyperbolic moveout equation. The robust moveout inversion ensures the flatness of wide-azimuth, long-spread events prior to stacking and amplitude picking. The moveout parameters also serve as the input to the anisotropic geometrical-spreading correction (Xu and Tsvankin, 2006a, 2006b) that should be applied prior to AVO analysis.

Far-offset amplitudes needed in our algorithm often are too low to make a meaningful contribution to the semblance operator. Therefore, it may be necessary to gain the whole data set as a prerequisite to stable AK semblance computation. This preprocessing step can be accomplished with any empirical gain function. As mentioned above, a more accurate geometrical-spreading correction can be applied after the moveout inversion.

In some of our tests for models with large velocity contrasts and class 1 AVO response, the critical angle was small enough for long-spread gathers to include postcritical offsets. As discussed by Landrø and Tsvankin (2007), the critical angle for orthorhombic media varies with azimuth and can be used in anisotropic parameter estimation. According to Sarkar et al. (2002), the phase change with offset at the critical angle does not lead to significant errors in stacking velocity when the hyperbolic moveout equation is used in the AK semblance computation. However, our numerical tests show that the wavelet distortions at postcritical angles sharply reduce the accuracy of η estimation. Indeed, the assumption of constant K within the semblance window implies that the wavelet shape does not change with offset. Therefore, it is essential to mute out postcritical offsets in nonhyperbolic AK semblance analysis.

Although the numerical examples here were generated for two-layer models, the AK semblance algorithm can be applied in the-

Table 4. Orthorhombic/orthorhombic model for which the P-wave reflection has an azimuthally varying class 2 AVO response. The two media have the same orientation of the vertical symmetry planes. Compared to the model from Table 3, the polarity reversal occurs at larger offsets.

	Layer 1	Layer 2
Symmetry type	ORTH	ORTH
Density (g/cm^3)	2.4	2.5
V_{P0} (km/s)	2.35	2.50
V_{S0} (km/s)	1.41	1.83
$\varepsilon^{(1)}$	0.20	0.16
$\delta^{(1)}$	0.08	0.09
$\gamma^{(1)}$	0.18	0.05
$\varepsilon^{(2)}$	0.13	0.09
$\delta^{(2)}$	−0.08	−0.07
$\gamma^{(2)}$	0.05	0.03
$\delta^{(3)}$	−0.08	−0.09
$V^{(1)}_{nmo}$	2.53	2.72
$V^{(2)}_{nmo}$	2.16	2.32
$\eta^{(1)}$	0.10	0.09
$\eta^{(2)}$	0.25	0.19
$\eta^{(3)}$	0.07	0.14

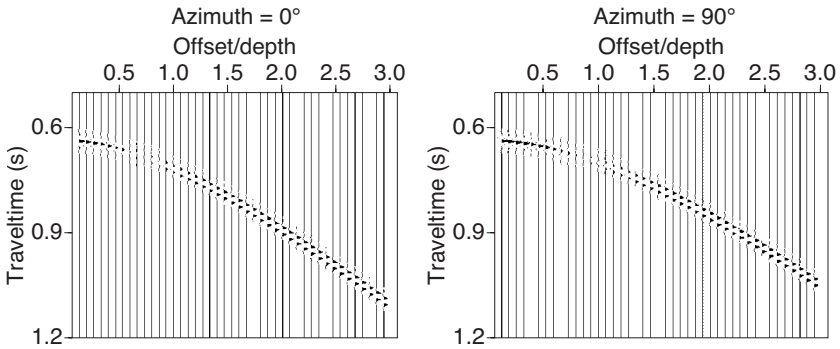

Figure 7. Shot records of a P-wave reflection from an orthorhombic/orthorhombic interface with a class 2 AVO response (Table 4). The seismograms are computed for the symmetry planes $[x_1,x_3]$ ($\alpha = 0°$) and $[x_2,x_3]$ ($\alpha = 90°$). The offset of the polarity reversal for this model varies noticeably with azimuth.

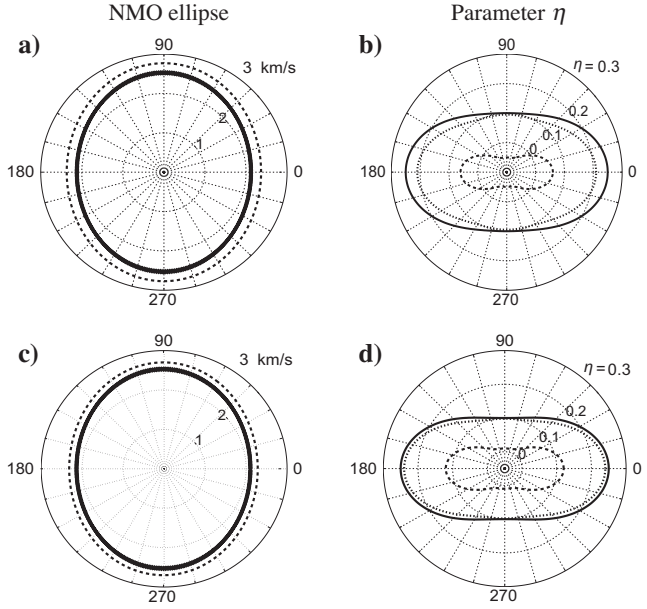

Figure 8. Moveout-inversion results for a wide-azimuth, long-offset P-wave reflection from an orthorhombic/orthorhombic interface (Table 4). The event has a class 2 AVO response with the polarity reversal at offsets between $x/h = 0.65$ and $x/h = 0.85$ (Figure 7). The maximum offset-to-depth ratio is two for the top row, and three for the bottom row. The solid lines are the actual NMO ellipses and η-curves, the dashed lines are estimated by the conventional semblance algorithm, and the dotted lines by AK semblance (the dotted and solid curves on plots [a] and [c] almost coincide).

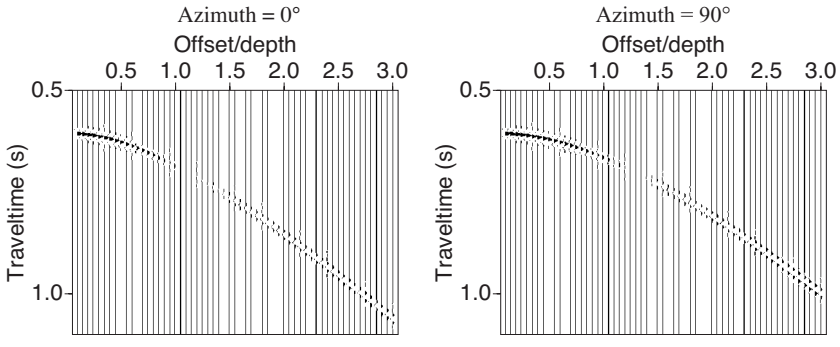

Figure 9. Shot records of a P-wave reflection from an orthorhombic/isotropic interface with a class 1 AVO response (Table 5). The seismograms are computed for the symmetry planes $[x_1,x_3](\alpha = 0°)$ and $[x_2,x_3](\alpha = 90°)$.

Table 5. Orthorhombic/isotropic model for which the P-wave reflection has an azimuthally varying class 1 AVO response.

	Layer 1	Layer 2
Symmetry type	ORTH	ISO
Density (g/cm^3)	2.4	2.6
V_{P0} (km/s)	3.30	3.84
V_{S0} (km/s)	1.45	2.46
$\varepsilon^{(1)}$	0.20	0
$\delta^{(1)}$	0.10	0
$\gamma^{(1)}$	0.20	0
$\varepsilon^{(2)}$	0.13	0
$\delta^{(2)}$	−0.10	0
$\gamma^{(2)}$	0.05	0
$\delta^{(3)}$	0.02	0
$V^{(1)}_{\rm nmo}$	3.61	3.84
$V^{(2)}_{\rm nmo}$	2.95	3.84
$\eta^{(1)}$	0.08	0
$\eta^{(2)}$	0.29	0
$\eta^{(3)}$	0.07	0

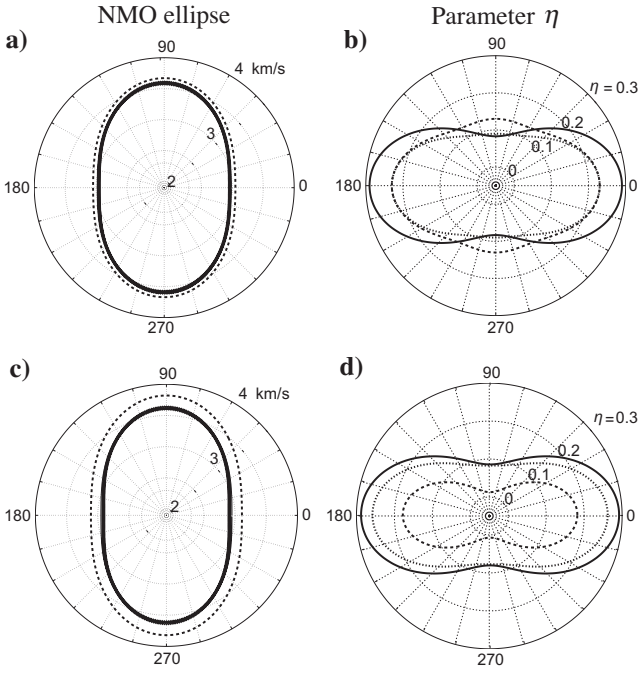

Figure 10. Moveout-inversion results for a wide-azimuth, long-offset P-wave reflection from an orthorhombic/isotropic interface (Table 5). The event has a class 1 AVO response with the polarity reversal at offsets between $x/h = 1$ and $x/h = 1.5$ (Figure 9). The maximum offset-to-depth ratio is two for the top row, and three for the bottom row. The solid lines are the actual NMO ellipses and η-curves, the dashed lines are estimated by the conventional semblance algorithm, and the dotted lines by AK semblance. As in Figure 8, the dotted and solid curves on plots (a,c) almost coincide.

same way to multilayered VTI and orthorhombic media. In the presence of vertical heterogeneity, the estimated moveout parameters represent effective quantities for the medium above the reflector (Vasconcelos and Tsvankin, 2006). Furthermore, the method can be used for more complicated, laterally heterogeneous subsurface models as long as the reflection moveout is adequately described by the nonhyperbolic moveout equation 7 with fitted coefficients. It should be mentioned, however, that AK semblance cannot help to resolve the trade-offs between the NMO velocities and η parameters discussed in detail by Tsvankin (2005) and Vasconcelos and Tsvankin (2006).

CONCLUSIONS

Polarity reversals, which may be quite common for long-offset reflection events, can produce significant distortions in velocity estimation using conventional semblance analysis. We have presented an efficient AVO-sensitive methodology designed to account for the influence of polarity reversals on moveout inversion for long-offset 2D and 3D (wide-azimuth) P-wave reflection data. The 2D algorithm is based on the Alkhalifah-Tsvankin nonhyperbolic moveout equation that accurately describes P-wave traveltimes in vertical symmetry planes of layered anisotropic media. Following the AK semblance method of Sarkar, Baumel, and Larner, amplitude variation with offset is approximated by a two-parameter function that reduces to Shuey's AVO equation when the overburden is isotropic and homogeneous. To minimize the trade-offs between the model parameters, the ratio of the AVO gradient and intercept ($K = B/A$) is kept constant for each reflection event.

Although the amplitude dependence employed in our method does not include geometrical spreading and higher-order AVO terms, it proved sufficiently accurate for moveout analysis. Synthetic tests on long-offset P-wave data from VTI media show that conventional semblance breaks down for class 2 AVO responses with the polarity reversal at relatively small (less than unity) offset-to-depth ratios. Even when combined with the Alkhalifah-Tsvankin equation, the conventional semblance operator produces errors in the NMO velocity and completely distorts the key time-processing parameter η. These errors are practically eliminated by the AK semblance operator, which achieves the same high accuracy in the estimates of $V_{\rm nmo}$ and η as that for AVO-free events.

Despite the addition of the amplitude parameters (A, which is defined at each time sample, and K), the 2D AK semblance algorithm is computationally efficient because the best-fit values of A and K are obtained analytically by differentiating the semblance function. As a result, the scanning is carried out over the same two moveout parameters ($V_{\rm nmo}$ and η) as in the conventional method. The only difference between the AK and conventional algorithms in terms of computational cost is in the more complicated form of the AVO-sensitive semblance operator.

For 3D wide-azimuth data, AK semblance needs to account for the azimuthally dependent offset of the polarity reversal. The amplitude function in our 3D AK semblance operator is based on the azimuthal variation of the AVO gradient for orthorhombic media, which is controlled by the symmetry-plane values of K ($K^{(1)}$ and $K^{(2)}$). This function was incorporated into a nonhyperbolic moveout inversion algorithm for wide-azimuth data that operates with a generalized form of the Alkhalifah-Tsvankin equation. The 3D AK semblance is designed to invert for $K^{(1)}$ and $K^{(2)}$ along with the moveout parameters of orthorhombic media, which include the azimuth of

one of the symmetry planes, two symmetry-plane NMO velocities ($V_{\rm nmo}^{(1)}$ and $V_{\rm nmo}^{(2)}$), and three η coefficients ($\eta^{(1,2,3)}$). To start the semblance search with an accurate initial model, the multidimensional scan on the full 3D gather is preceded by estimation of the NMO ellipse and by 2D inversion of long-offset data near the symmetry-plane directions.

The improvement achieved by the 3D AK semblance is especially significant for orthorhombic models with class 2 AVO response. Because the polarity reversal occurs at small offsets, the conventional method completely breaks down and may even produce η values that have the wrong sign. Despite the approximate nature of its amplitude function, the AK semblance algorithm properly accounts for the azimuthally varying polarity reversal in the estimation of both the NMO ellipse and the parameters $\eta^{(1,2,3)}$. For class 1 AVO, the polarity reversal occurs at larger offsets (typically, at offset-to-depth ratios larger than unity), which makes the conventional method more accurate. Still, inversion for the η-parameters requires offsets reaching at least two reflector depths, so the polarity reversal distorts the output of the conventional semblance operator. In contrast to AK semblance, for class 1 AVO the conventional algorithm produces larger errors in $\eta^{(1,2,3)}$ with increasing spreadlength as the influence of the polarity reversal becomes more substantial.

On the whole, nonhyperbolic moveout inversion for both class 1 and class 2 AVO response should be performed with the AVO-sensitive semblance operator. Although it may be possible to reconstruct the NMO ellipse by applying conventional semblance to a truncated gather (mostly for class 1 AVO), accurate estimation of the η-parameters requires application of AK semblance. Note that in combination with the NMO velocities $V_{\rm nmo}^{(1)}$ and $V_{\rm nmo}^{(2)}$, the parameters $\eta^{(1,2,3)}$ control time processing and geometrical spreading of P-wave data in orthorhombic media.

ACKNOWLEDGMENTS

We are grateful to members of the A(nisotropy)-Team of the Center for Wave Phenomena (CWP), Colorado School of Mines (CSM), for helpful discussions. We would like to thank Debashish Sarkar (GX Technology) and Ivan Vasconcelos (CSM; now at GX Technology) for providing their codes, which were critically important for the success of this study. The suggestions of Brian Macy (ConocoPhillips), Debashish Sarkar, and an anonymous reviewer helped to improve the manuscript. This work was supported by the Consortium Project on Seismic Inverse Methods for Complex Structures at CWP and by the Chemical Sciences, Geosciences and Biosciences Division, Office of Basic Energy Sciences, Office of Science, U. S. Department of Energy.

APPENDIX A

THE 2D AND 3D AK SEMBLANCE OPERATORS

AK semblance in 2D

Conventional semblance operators are based on summation of trace amplitudes along moveout curves (which usually are hyperbolic) within a certain time window. The idea of amplitude-sensitive semblance is to replace this summation with data modeling using a moveout equation in combination with an amplitude function $M(t_1,x)$, where t_1 is the zero-offset time and x is the source-receiver offset. The amplitude function for AK semblance is specified as (Sarkar et al., 2002)

$$M(t_1,x) = A(t_1)(1 + K\sin^2\theta_x), \tag{A-1}$$

where $A(t_1)$ is the AVO intercept, K is the ratio of AVO gradient and intercept (K is kept constant inside the semblance window), and θ_x is the incidence angle at the reflector, approximately given by

$$\sin^2\theta_x = \frac{x^2}{x^2 + t_0^2 V_{\rm nmo}^2}; \tag{A-2}$$

$V_{\rm nmo}$ is the NMO velocity and t_0 is the zero-offset time at the center of the semblance window.

Following Sarkar et al. (2002), we define the 2D AK semblance operator as

$$S_G(t_0) = 1 - \frac{\sum_{t_1}\sum_{x}[A(t_1)(1 + K\sin^2\theta_x) - D_V(t_1,x)]^2}{\sum_{t_1}\sum_{x} D_V^2(t_1,x)}, \tag{A-3}$$

where $D_V = D_V(t_1,x)$ is the moveout-corrected data at the zero-offset time t_1; the summation is carried out over all offsets x and all time samples within the semblance window centered at t_0. The subscript V denotes the trial NMO velocity $V_{\rm nmo}$ used by Sarkar et al. (2002) to perform the conventional hyperbolic moveout correction. In our algorithm, the data are modeled using a nonhyperbolic moveout equation parameterized by $V_{\rm nmo}$ and the anellipticity coefficient η (see the main text).

The value of the AVO intercept that corresponds to the maximum of the generalized semblance function can be found by setting to zero the derivative of equation A-3 with respect to $A(t_1)$:

$$A(t_1) = \frac{\sum_{x}[D_V(t_1,x)(1 + K\sin^2\theta_x)]}{\sum_{x}(1 + K\sin^2\theta_x)^2}. \tag{A-4}$$

Substituting $A(t_1)$ from equation A-4 into equation A-3 yields

$$S_G(t_0) = \frac{\sum_{t_1}\left[\sum_{x} D_V(t_1,x)(1 + K\sin^2\theta_x)\right]^2}{\sum_{x}(1 + K\sin^2\theta_x)^2 \sum_{t_1}\sum_{x} D_V^2(t_1,x)}. \tag{A-5}$$

Similarly, next we differentiate S_G (equation A-5) with respect to K and set the derivative to zero:

$$\mu K^2 - \beta K + \gamma = 0, \tag{A-6}$$

where

$$\mu = \sum_{x}\sin^2\theta_x \sum_{t_1}\left(\sum_{x} D_V(t_1,x)\sin^2\theta_x\right)^2 - \sum_{x}\sin^2\theta_x \sum_{t_1}\left[\sum_{x} D_V(t_1,x)\sum_{x}(D_V(t_1,x)\sin^2\theta_x)\right], \tag{A-7}$$

$$\beta = \sum_{x}\sin^2\theta_x \sum_{t_1}\left(\sum_{x} D_V(t_1,x)\right)^2 - N\sum_{t_1}\left(\sum_{x} D_V(t_1,x)\sin^2\theta_x\right)^2, \tag{A-8}$$

and

$$\gamma = N\sum_{t_1}\left[\sum_x D_V(t_1,x)\sum_x (D_V(t_1,x)\sin^2\theta_x)\right] - \sum_x \sin^2\theta_x \sum_{t_1}\left(\sum_x D_V(t_1,x)\right)^2. \quad \text{(A-9)}$$

The solution of the quadratic equation A-6 that maximizes the semblance for both positive and negative values of μ is (Sarkar et al., 2002)

$$K = \frac{\beta - \sqrt{\beta^2 - 4\mu\gamma}}{2\mu}. \quad \text{(A-10)}$$

Substituting K from equation A-10 into equation A-5, we obtain the 2D generalized semblance operator that depends only on the parameters of the moveout function.

AK semblance in 3D

Here, the AK semblance operator is extended to long-offset 3D data collected into CMP gathers with a wide range of source-receiver azimuths. The 3D AK semblance is computed from equation A-3, where the summation is performed not only over all offsets x but also over all azimuths α. Setting the derivative of $S_G(t_0)$ with respect to $A(t_1)$ to zero, we obtain the generalized 3D semblance in a form similar to equation A-5:

$$S_G(t_0) = \frac{\sum_{t_1}\left[\sum\sum_{x\ \alpha} D_V(t_1,x,\alpha)\,(1 + K(\alpha)\sin^2\theta_x)\right]^2}{\sum\sum_{x\ \alpha}(1 + K(\alpha)\sin^2\theta_x)^2 \sum\sum\sum_{t_1\ x\ \alpha} D_V^2(t_1,x,\alpha)}. \quad \text{(A-11)}$$

The incidence angle θ_x is found from equation A-2 with azimuthally varying NMO velocity:

$$\sin^2\theta_x = \frac{x^2}{x^2 + t_0^2 V_{\mathrm{nmo}}^2(\alpha)}. \quad \text{(A-12)}$$

As discussed in the main text, the function $K(\alpha)$ is based on the azimuthal dependence of the AVO gradient in orthorhombic media:

$$K(\alpha) = K^{(1)}\sin^2(\alpha - \varphi) + K^{(2)}\cos^2(\alpha - \varphi), \quad \text{(A-13)}$$

where φ is the azimuth of the $[x_1,x_3]$ symmetry plane. Therefore, in the 3D case, the normalized gradient K is defined by two independent parameters ($K^{(1)}$ and $K^{(2)}$), which are difficult to obtain analytically. Instead, $K^{(1)}$ and $K^{(2)}$ are estimated from the semblance scan using equation A-11. Assuming that the model is orthorhombic, we use the generalized Alkhalifah-Tsvankin nonhyperbolic moveout equation parameterized by the azimuth φ, the symmetry-plane NMO velocities $V_{\mathrm{nmo}}^{(1)}$ and $V_{\mathrm{nmo}}^{(2)}$, and the anellipticity coefficients $\eta^{(1)}$, $\eta^{(2)}$, and $\eta^{(3)}$. Therefore, semblance scanning is performed over a total of eight independent parameters, as discussed in more detail in the main text.

REFERENCES

Alkhalifah, T., and I. Tsvankin, 1995, Velocity analysis for transversely isotropic media: Geophysics, **60**, 1550–1566.

Bakulin, A., V. Grechka, and I. Tsvankin, 2000, Estimation of fracture parameters from reflection seismic data — Part II: Fractured models with orthorhombic symmetry: Geophysics, **65**, 1803–1817.

Biondi, B. L., and C. Kostov, 1989, High-resolution velocity spectra using eigenstructure methods: Geophysics, **54**, 832–842.

Corcoran, C. T., and A. J. Seriff, 1993, Methods for processing seismic data: U. S. Patent 5 197 039; European Patent 335–450.

Gajewski, D., and I. Pšenčík, 1987, Computation of high frequency seismic wavefields in 3-D laterally inhomogeneous anisotropic media: Geophysical Journal of the Royal Astronomical Society, **91**, 383–412.

Grechka, V., and M. Kachanov, 2006, Seismic characterization of multiple fracture sets: Does orthotropy suffice?: Geophysics, **71**, no. 3, D93–D105.

Key, S. C., and S. B. Smithson, 1990, New approach to seismic-reflection event detection and velocity determination: Geophysics, **55**, 1057–1069.

Kim, K. Y., K. H. Wrolstad, and F. Aminzadeh, 1993, Effects of transverse isotropy on P-wave AVO for gas sands: Geophysics, **58**, 883–888.

Landrø, M., and I. Tsvankin, 2007, Seismic critical-angle reflectometry: A method to characterize azimuthal anisotropy?: Geophysics, **72**, no. 3, D41–D50.

Pech, A., and I. Tsvankin, 2004, Quartic moveout coefficient for a dipping azimuthally anisotropic layer: Geophysics, **69**, 699–707.

Press, W. H., S. A. Teukolsky, W. T. Vetterling, and B. P. Flannery, 1992, Numerical Recipes in C: The art of scientific computing: Cambridge University Press.

Rüger, A., 2001, Reflection coefficients and azimuthal AVO analysis in anisotropic media: SEG.

Rutherford, S., and R. Williams, 1989, Amplitude-versus-offset variations in gas sands: Geophysics, **54**, 680–688.

Sarkar, D., R. T. Baumel, and K. Larner, 2002, Velocity analysis in the presence of amplitude variation: Geophysics, **67**, 1664–1672.

Sarkar, D., J. P. Castagna, and W. Lamb, 2001, AVO and velocity analysis: Geophysics, **66**, 1284–1293.

Schoenberg, M., and K. Helbig, 1997, Orthorhombic media: Modeling elastic wave behavior in a vertically fractured earth: Geophysics, **62**, 1954–1974.

Shuey, R. T., 1985, A simplification of the Zoeppritz equations: Geophysics, **50**, 609–614.

Symes, W. W., and M. Kern, 1994, Inversion of reflection seismograms by the differential semblance analysis: Algorithm structure and synthetic examples: Geophysical Prospecting, **42**, 565–614.

Taner, M. T., and F. Koehler, 1969, Velocity spectra-digital computer derivation and applications of velocity functions: Geophysics, **34**, 859–881.

Thomsen, L., 1986, Weak elastic anisotropy: Geophysics, **51**, 1954–1966.

Tsvankin, I., 1997, Anisotropic parameters and P-wave velocity for orthorhombic media: Geophysics, **62**, 1292–1309.

——–, 2005, Seismic signatures and analysis of reflection data in anisotropic media: 2nd ed., Elsevier Science.

Tsvankin, I., and L. Thomsen, 1994, Nonhyperbolic reflection moveout in anisotropic media: Geophysics, **59**, 1290–1304.

Vasconcelos, I., and I. Tsvankin, 2006, Non-hyperbolic moveout inversion of wide-azimuth P-wave data for orthorhombic media: Geophysical Prospecting, **54**, 535–552.

Xu, X., and I. Tsvankin, 2006a, Anisotropic geometrical-spreading correction for wide-azimuth P-wave reflections: Geophysics, **71**, no. 5, D161–D170.

——–, 2006b, Azimuthal AVO analysis with anisotropic spreading correction: A synthetic study: The Leading Edge, **24**, 1336–1342.